Attosecond double-ionization dynamics of aligned H_2: Two-dimensional quantum simulations

Shang Wang and Yanjun Chen*
College of Physics and Information Technology, Shaan'xi Normal University, Xi'an, China
(Received 7 January 2015; published 20 August 2015)

A fully quantum procedure, based on the numerical solution of the time-dependent Schrödinger equation (TDSE) with two spatial dimensions for every electron, is developed to study the attosecond double-ionization (DI) dynamics from aligned H_2 molecules in strong laser fields. Our simulations are able to reproduce the orientation dependence of DI, as observed for N_2 in experiments [D. Zeidler *et al.*, Phys. Rev. Lett. **95**, 203003 (2005)]. Our TDSE analyses reveal the important roles of the lateral motion of the electron and two-center interference in the orientation-dependent DI. Our results give suggestions on the ultrafast probing of the dynamics of DI from aligned molecules.

DOI: 10.1103/PhysRevA.92.023418 PACS number(s): 33.80.Rv, 31.70.Hq

I. INTRODUCTION

In strong-laser-matter interaction, the electron rescattering [1] can lead to many interesting physical phenomena such as high-order-harmonic generation (HHG) [2–5], high-order above-threshold ionization (HATI) [6–8], and nonsequential double ionization (NSDI) [9–13]. In comparison with HHG and HATI, the physical phenomena for NSDI are richer and have attracted great interests in recent years [14–21]. In particular, as the orientation of the molecule [22–25] is considered, some new effects emerge.

The experimental studies of N_2 [26] have found that the two electrons involved in NSDI more likely exit the molecule in the same (opposite) direction for $\theta = 0^\circ$ (90°; θ is the angle between the molecular axis and the laser polarization). As the intricate phenomena are expected to be associated with the geometry structure of the aligned molecule, the details of the interplay of the molecular structure and the electron dynamics remain unknown so far. To understand these phenomena, a theoretical analysis is highly desired. However, the theoretical treatment of the NSDI from aligned molecules encounters difficulty. As the well-known strong-field approximations (SFAs) [27,28] have explained many NSDI-related phenomena, the SFA neglects the Coulomb and multiphoton effects, which have been shown to be important in NSDI [26,29]. On the other hand, the numerical study of the NSDI from aligned molecules such as H_2 [30–32], based on the time-dependent Schrödinger equation (TDSE), is limited by the high-dimension simulations involved in the theoretical description of two-electron dynamics.

In addition, the experimental studies of H_2 also show that the molecular orientation can play an important role in the dynamics of NSDI [33]. For example, the experimental measurements suggest that the transverse velocity spread of the electron related to the lateral motion is smaller for the perpendicular molecule than the parallel one. This phenomenon is responsible for different ellipticity dependences of NSDI at different orientation angles. To understand this phenomenon, a detailed theoretical study of the orientation dependence of the molecular NSDI is also needed.

In this paper, by developing applicable numerical schemes, we study the NSDI of aligned H_2 through the numerical solution of the TDSE. We use a two-dimensional (2D) two-electron model with every electron having two degrees of freedom: parallel and perpendicular to the laser polarization. Our simulations reproduce the angle dependence of NSDI, as observed for N_2 [see Figs. 4(c) and 4(d) below]. Our TDSE analyses allow us to access the rescattering event for aligned molecules in the atomic space-time scale. Our simulations show that due to the geometrical structure of the molecule, the electrons more easily evade each other laterally (longitudinally) for the parallel (perpendicular) orientation, resulting in different responses of NSDI to the molecular orientation. The angle dependence of NSDI is also influenced highly by the effect of two-center interference and is sensitive to the laser intensity. Our results open new perspectives for the study of NSDI from aligned molecules.

This paper is organized as follows. We introduce the numerical method in Sec. II. In Sec. III, we show our numerical results for the orientation dependence of single-ionization and double-ionization yields, showing the ratio of double- vs single-ionization yields is larger for the perpendicular molecule than the parallel one. The possible physical mechanisms for the orientation dependence of NSDI are analyzed in Sec. IV. The important influence of the lateral motion of the electron on the angle-dependent NSDI is also addressed there. The role of two-center interference in NSDI from aligned molecules is discussed in Sec. V. Extended discussions on different NSDI mechanisms arising from rescattering are presented in Sec. VI. Sec. VII is our conclusion.

II. NUMERICAL METHOD

The 2D two-electron Hamiltonian in the Born-Oppenheimer (BO) approximation studied here has the following form (in atomic units of $\hbar = e = m_e = 1$):

$$H(t) = \sum_{i=1}^{2}[H_{0i} + \mathbf{E}(t)\cdot\mathbf{r}_i] + \frac{1}{\sqrt{(\mathbf{r}_1 - \mathbf{r}_2)^2 + \varepsilon}}. \quad (1)$$

Here, $H_{0i} = \frac{\mathbf{p}_i^2}{2} - \frac{Z}{\sqrt{r_{1i}^2+\varepsilon}} - \frac{Z}{\sqrt{r_{2i}^2+\varepsilon}}$ is the single-electron Hamiltonian, with $r_{1i}^2 = (x_i - \frac{R}{2}\cos\theta)^2 + (y_i - \frac{R}{2}\sin\theta)^2$ and $r_{2i}^2 = (x_i + \frac{R}{2}\cos\theta)^2 + (y_i + \frac{R}{2}\sin\theta)^2$. $\mathbf{r}_i$ is the electron's

*chenyjhb@gmail.com

coordinate, and $\varepsilon = 0.5$ is the smoothing parameter which is used to handle the singularity when $\mathbf{r}_1 = \mathbf{r}_2$. $Z = 1$ is the effective charge, and $R = 1.4$ a.u. is the internuclear distance. $\mathbf{E}(t) = -\vec{\mathbf{e}}_x f(t) E \sin\omega_0 t$ is the external electric field, with E being the amplitude and ω_0 being the frequency. $\vec{\mathbf{e}}_x$ is the unit vector along the x axis, and $f(t)$ is the envelope function.

It should be mentioned that for the real system, the internuclear separation is about 1.4 a.u. for H_2, but it is about 1.9 a.u. for H_2^+. The effective charges at these corresponding internuclear separations are about 1.25 for H_2 and 1.31 for H_2^+. These parameters are somewhat different from those used in this paper for the 2D model H_2 molecule with the BO approximation. In addition, in our 2D model, the laser field is polarized in the 2D plane, and the propagation direction of the laser field is neglected. The latter implies that the influence of the Lorentz force of the magnetic field is also not considered in our simulations. As discussed in Ref. [34], due to this Lorentz force, the electron is moved an amount $\Delta z = (2\pi/c\omega_0)U_p$ along the propagation direction of the laser field. Here, $U_p = E^2/(4w_0^2)$ is the ponderomotive energy, and c is the velocity of light. The effect of the magnetic field becomes remarkable for a laser intensity higher than 10^{15} W/cm^2. For the case of 800-nm, 2×10^{14} W/cm^2 laser light studied in this paper, $\Delta z \approx 0.36$ a.u., which is small and suggests that the effect of the magnetic field is not significant here.

The 2D model has been used in the theoretical study of the HHG from aligned H_2^+ molecules [3] and has been shown to hold the essence of the physics of the process when it is compared with three-dimensional (3D) results [35]. We expect that as the laser field is not very strong, the main results obtained from our 2D simulations will also hold in 3D cases. For strong laser fields at which the effect of the magnetic field is remarkable, a 3D model is desired.

The ground-state wave function $|\phi_0(\mathbf{r}_1,\mathbf{r}_2)\rangle$ and the corresponding energy $E_0(H_2)$ of the two-electron field-free Hamiltonian $H_0 = \sum_{i=1}^{2} H_{0i} + 1/\sqrt{(\mathbf{r}_1-\mathbf{r}_2)^2+\varepsilon}$ are evaluated numerically by propagating the Schrödinger equation in imaginary time [36,37]. Once $|\phi_0(\mathbf{r}_1,\mathbf{r}_2)\rangle$ and $E_0(H_2)$ are obtained, we can evaluate the ground-state energy $E_0(H_2^{2+})$ for the single-electron Hamiltonian H_{0i} through $E_0(H_2^{2+}) = \langle\phi_0|H_{0i}|\phi_0\rangle$. The one-electron binding energy $E_0(e)$ associated with the total electronic energy of the model H_2 molecule can be obtained with $E_0(e) = E_0(H_2) - E_0(H_2^{2+})$. With the above treatments, the ground-state electronic energies (which do not include nuclear repulsion and vibration energy) obtained here are $E_0(H_2) = -1.83$ a.u. and $E_0(H_2^{2+}) = -1.19$ a.u. The one-electron binding energy obtained is $E_0(e) = -0.64$ a.u. These values are close to the real ones.

In our calculations, we use ten-cycle laser pulses with a $\sin^2$-shaped envelop function. Numerically, the TDSE of $H(t)$ is solved with the spectral method [38]. The 2D simulations of a two-electron system of H_2, involving four degrees of freedom, are very time-memory consuming. Here, we work with a grid size of 110×55 a.u. for the x and y axes of every electron, respectively. The grid spacing at these axes is $\triangle = 0.86$ a.u., and the time step in the TDSE is 0.067 a.u. The laser wavelength used here is $\lambda = 800$ nm, and we have explored a laser-intensity region of $I = 0.25 \times 10^{14}$ to 2×10^{14} W/cm^2. For $I = 2 \times 10^{14}$ W/cm^2, the maximal classical momentum involved in our calculations is $E/w_0 \approx 1.33$ a.u., and the maximal kinetic energy of the rescattering electron is $3.17U_p \approx 1.4$ a.u. These can easily be represented on our numerical grid. A parallel code is developed to accelerate the calculation, and the numerical convergence is checked by increasing the grid. After each time step the TDSE wave function $\psi(x_1,y_1,x_2,y_2,\theta,t)$ of $H(t)$ is multiplied by a mask function to absorb the continuum wave packet at the boundary. These absorbed wave packets $\int |\psi_f(x_1,y_1,x_2,y_2,\theta,t)|^2 dt$, with $r_1 = \sqrt{x_1^2+y_1^2} < 8$ a.u. or $r_2 = \sqrt{x_2^2+y_2^2} < 8$ a.u. [15], are defined as the single-ionization (SI) yields; others are defined as the double-ionization (DI) yields at the angle θ. To get an overall view of the molecular DI, below we will first discuss the angle-dependent SI and DI yields.

III. SI AND DI YIELDS AT DIFFERENT ANGLES

In Fig. 1(a), we show the ratios of SI (curve with black squares) and DI (the curve with red circles) yields at $\theta = 0^\circ$ vs $\theta = 90^\circ$ with varying laser intensities. As one can see from Fig. 1(a), the ratio for SI is always larger than unity, which implies that the SI has a stronger preference for the parallel orientation [39]. This preference diminishes with the increase of the laser intensity. However, the situation is very different for DI. The ratio for DI can be smaller than unity at lower laser intensities, and on the whole it increases as the laser intensity increases. These comparisons show that the SI and DI of the two-electron system respond differently to the angle θ, especially for lower laser intensities. According to the SFA [27], the SI is closely associated with the tunneling process in which the structure of the molecule is distorted significantly by the laser field [39]. The DI, however, is related to not only tunneling but also the recollision process, in which the molecular structure can play a more important role than in tunneling [28,40].

The DI yields $D(\theta)$ at the angle θ can be denoted simply using $D(\theta) \sim S(\theta)R(\theta)$. Here, $S(\theta)$ is the SI yields, and $R(\theta)$ is the amplitude for the recollision of the rescattering electron with the second electron. From the above expression, we can approximate the amplitude $R(\theta)$ using $R(\theta) \sim D(\theta)/S(\theta)$, i.e., the amplitude can be considered the ratio of DI vs SI yields. In Fig. 1(b), we plot the ratio of DI vs SI yields at $\theta = 0^\circ$ and $\theta = 90^\circ$. Despite these different responses of DI and SI to the angle θ discussed in Fig. 1(a), the ratio of DI vs SI yields in Fig. 1(b) for different laser intensities is always larger at $\theta = 90^\circ$ than

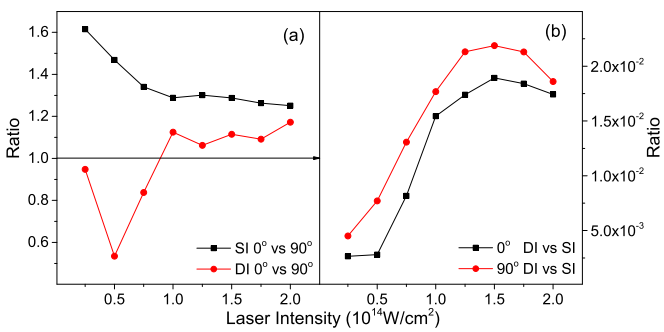

FIG. 1. (Color online) (a) The ratios of SI and DI yields at $\theta = 0^\circ$ vs $\theta = 90^\circ$ and (b) the ratios of DI vs SI yields at $\theta = 0^\circ$ and 90° for model H_2 with different laser intensities.

that at $\theta = 0^\circ$. We thus conclude that the recollision amplitude $R(\theta)$, which can be expected to be closely associated with the cross section, is larger in the perpendicular orientation than the parallel one.

Recent studies have shown that the cross section for the parallel molecule is larger than the perpendicular one [41–43], in significant disagreement with our results. To explain the uncommon phenomena, next, we turn to the momentum distribution of the system. We mention that the ratio of DI vs SI yields presented here is also several orders of magnitude larger than the ionization probability of a 2D H_2^+ molecular ion calculated in our extended simulations. This result is similar to that in Ref. [15] and implies that for the present parameter region, the NSDI related to rescattering dominates in the DI.

IV. EFFECTS AFFECTING MOMENTUM DISTRIBUTIONS

In this section, our discussions will focus on the three typical cases of $I = 0.5 \times 10^{14}, 1.25 \times 10^{14}$, and 2×10^{14} W/cm^2, corresponding to low, intermediate, and high laser intensities for the NSDI, as shown in Fig. 1(a). We restrict our analysis to snapshots of the momentum distribution $|\phi|^2$. Here, the momentum wave function $\phi \equiv \phi(p_{1x}, p_{1y}, p_{2x}, p_{2y}, \theta, t_m)$ is evaluated using the Fourier translation of the TDSE wave function $\psi(x_1, y_1, x_2, y_2, \theta, t_m)$, with $r_{1,2} = \sqrt{x_{1,2}^2 + y_{1,2}^2} > 8$ a.u. at the time $t_m = 5.25T$ ($T = 2\pi/\omega_0$ is the laser cycle). For this time at which the laser field $\mathbf{E}(t)$ is maximal and the vector potential $\mathbf{A}(t)$ of $\mathbf{E}(t)$ is zero, the snapshot of the momentum distribution can then be considered the final momentum distribution of the process [15]. The two-electron momentum distribution along the laser polarization $|\phi_\parallel(p_{1x}, p_{2x}, \theta, t_m)|^2$ is then obtained through the integral of $|\phi|^2$ over the perpendicular momenta p_{1y} and p_{2y}. Similarly, the corresponding single-electron momentum distribution $|\phi_1(p_{1x}, p_{1y}, \theta, t_m)|^2$ is then obtained with the integral of $|\phi|^2$ over the second-electron momenta p_{2x} and p_{2y}.

A. Low-intensity cases

In Figs. 2(a) and 2(b), we plot the two-electron momentum distributions parallel to the laser polarization $|\phi_\parallel|^2$ at $\theta = 0^\circ$ and $\theta = 90^\circ$. As one can see, the difference in the distributions in Figs. 2(a) and 2(b) is obvious. This distribution at $\theta = 0^\circ$ in Fig. 2(a) shows larger amplitudes around the diagonal of $p_{1x} = p_{2x}$ in quadrant 1, whereas the distribution in Fig. 2(b) for the perpendicular orientation shows somewhat larger amplitudes in quadrants 2 and 4. To highlight this difference, we also show the relative momentum distributions of $|\phi_\parallel(0^\circ)|^2 - |\phi_\parallel(90^\circ)|^2$ in Fig. 2(c) and $|\phi_\parallel(90^\circ)|^2 - |\phi_\parallel(0^\circ)|^2$ in Fig. 2(d), while setting all negative values to zero. Again, in Fig. 2(d), one can see the increase in probabilities in quadrants 2 and 4; in Fig. 2(c), the two electrons show a preference to exit the molecular potential with similar momenta in quadrant 1. Another important difference observed in quadrant 1 is that the distribution comprises mainly smaller momenta in Fig. 2(c), and it is made up of mainly larger momenta in Fig. 2(d).

For $I = 0.5 \times 10^{14}$ W/cm^2, the maximal return energy of the rescattering electron is 0.35 a.u., which is far from

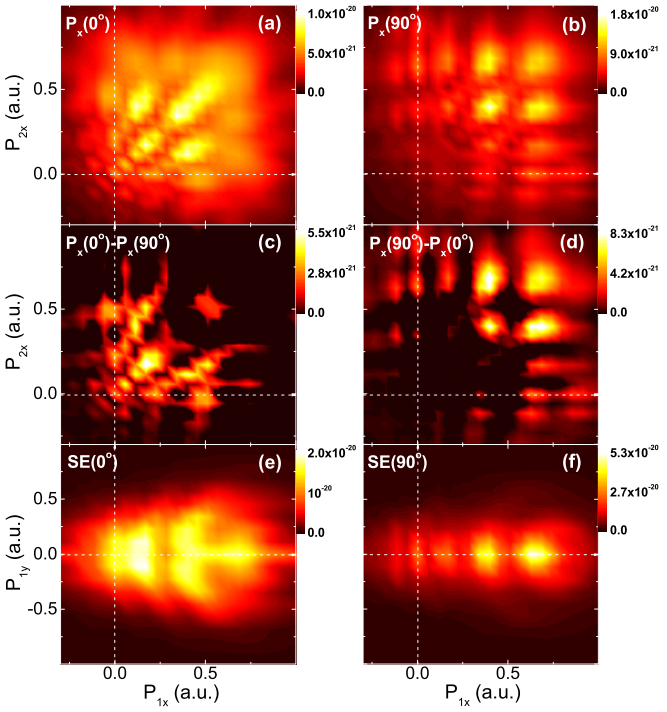

FIG. 2. (Color online) Longitudinal momentum distributions of model H_2 at (a) $\theta = 0^\circ$ and (b) $\theta = 90^\circ$. In (c) and (d), we show the longitudinal momentum distributions at $\theta = 0^\circ$ (90°) after subtracting that at $\theta = 90^\circ$ (0°), and all negative values have been set to zero. In (e) and (f), the single-electron (SE) momentum distributions at $\theta = 0^\circ$ and $\theta = 90^\circ$, respectively, are also shown. The laser intensity is $I = 0.5 \times 10^{14}$ W/cm^2. One can see that the maximal kinetic energy of the electron parallel to the laser polarization is about 0.27 a.u. for both $\theta = 0^\circ$ and 90° [see (a) and (b)]. That perpendicular to the laser polarization is about 0.11 a.u. for $\theta = 0^\circ$ [see (e)] and about 0.02 a.u. for $\theta = 90^\circ$ [see (f)].

the ionization potential of H_2^+. In this situation, one can expect that the recollision near zero field will induce doubly excited states of the aligned molecule. These two excited electrons are then ionized in rapid succession by the increasing field and their mutual repulsion within the attosecond time scale [29]. This is the case seen in Fig. 2(a) for the parallel molecule. Considering the Coulomb repulsion, the preference of escape of similar parallel momenta revealed in Fig. 2(a) also implies that at $\theta = 0^\circ$, these two electrons tend to evade each other through the motion perpendicular to the laser polarization. This tendency is checked in Figs. 2(e) and 2(f), where we plot the single-electron momentum distribution $|\phi_1|^2$. Indeed, one can see that the distribution in Fig. 2(e) shows large amplitudes around $p_{1y} = \pm 0.2$ a.u. and is remarkably broader than that in Fig. 2(f). The latter shows large amplitudes around the axis of $p_{1y} = 0$. From the comparisons in Fig. 2 we can now conclude that the two electrons prefer to evade each other laterally for the parallel orientation and longitudinally for the perpendicular orientation. The reason can be explained as follows. For the perpendicular molecule, after recollision, the electron with a nonzero lateral momentum will have to go through one of the two nuclei as it escapes, and the strong Coulomb-focusing effect [29] will keep it from leaving. The effect is weak for the parallel molecule. A sketch of the electron

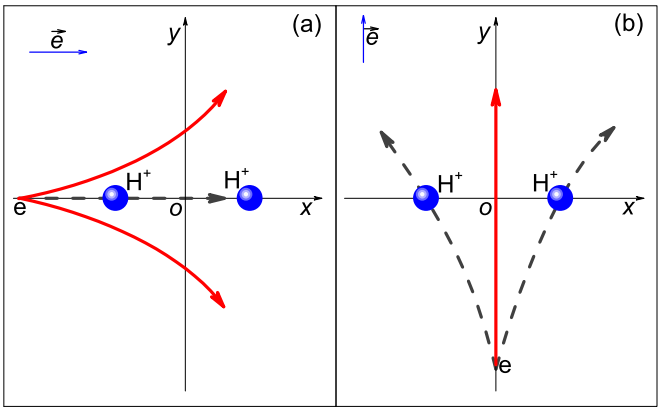

FIG. 3. (Color online) A sketch of the electron motion after recollision for the laser polarization $\vec{\mathbf{e}}$ (a) parallel or (b) perpendicular to the molecular axis, which is along the x axis here. The center of mass of the molecular system agrees with the origin of the coordinate system o. The red solid lines indicate the preferred route of the electron e as it escapes from the nuclei, H^+. The gray dashed lines indicate the avoided one along which the electron can collide with and therefore be captured by the nuclei. For the parallel case in (a), to avoid colliding with the nuclei, a small rescattering angle of the electron and thus a lateral velocity spread are expected, which is different from the perpendicular case in (b).

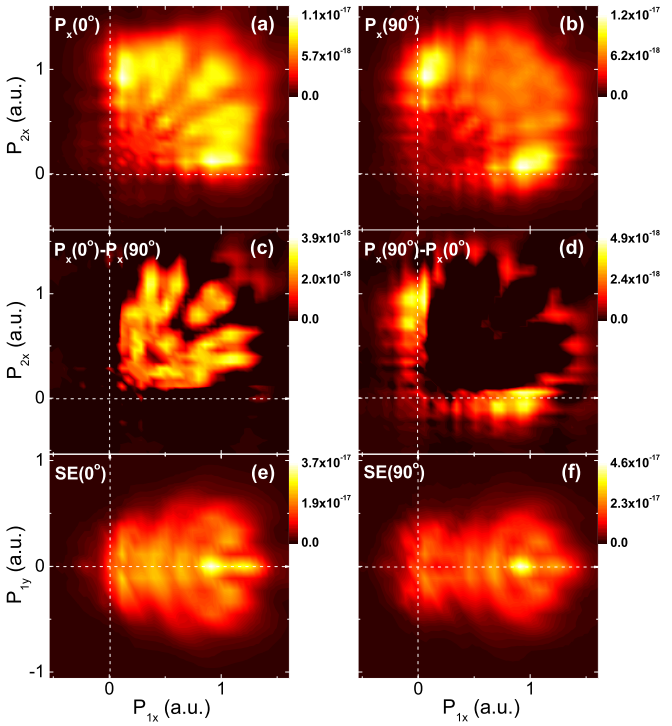

FIG. 4. (Color online) Same as Fig. 2, except $I = 1.25 \times 10^{14}$ W/cm^2. One can see that the maximal kinetic energy of the electron parallel to the laser polarization is about 0.75 a.u. for both $\theta = 0°$ and $90°$ [see (a) and (b)]. That perpendicular to the laser polarization is about 0.11 a.u. for $\theta = 0°$ [see (e)] and about 0.09 a.u. for $\theta = 90°$ [see (f)].

motion at different angles θ is presented in Fig. 3. We note that the smaller lateral velocity spread of the electron for the perpendicular molecule than for the parallel one, revealed here, is also in agreement with the experimental results discussed in Ref. [33].

Due to this preference, at $\theta = 0°$, the two electrons more easily stay in a doubly excited state (DES) as the field is near zero, and they are then ionized through tunneling as the field $\mathbf{E}(t)$ increases remarkably. In this case, the two electrons will be ejected with similar and smaller parallel momenta and differ from each other with regard to the perpendicular momenta. Similarly, due to this preference, at $\theta = 90°$, the DI more easily occurs through the direct recollision ionization (DRI) [1] or the recollision excitation followed by delayed tunnel ionization (REDTI) [44]. For the case of DRI, the rescattering electron collides and shares its energy with the second electron near zero field. This recollision frees the second electron, and both electrons are then ejected together with larger but somewhat different drift momenta, appearing in quadrant 1. For the case of REDTI, the recollision excites the second electron instead of freeing it directly; the second electron is then ionized as the field increases. In this case, the two electrons will exit the molecule in different directions and have momenta with opposite signs, appearing in quadrants 2 and 4. The above analyses explain the difference in the momentum distributions of the parallel vs perpendicular molecules observed in Fig. 2.

We mention that the distribution in Fig. 2(b) also shows some interference structures. Our other calculations show that the details of the interference structures are very sensitive to the laser intensity. We therefore expect that these interference structures arise from multiphoton effects which depend strongly on the laser parameter. Similar interference structures in the DI momentum distributions are also observed in other papers [17]. As these interference structures are sensitive to the laser intensity, they are not easy to understand and deserve detailed study in the future. As the laser intensity increases, the difference in the NSDI dynamics between $\theta = 0°$ and $\theta = 90°$ becomes clearer, as shown in Fig. 4.

B. Intermediate-intensity cases

For $I = 1.25 \times 10^{14}$ W/cm^2, the maximal return energy of the rescattering electron is 0.9 a.u., which is near the ionization potential of H_2^+. In this case, one can expect the DRI or REDTI mechanism will dominates in DI. Indeed, in Figs. 4(a) and 4(b), one can see that the distributions have larger amplitudes off the diagonal in quadrant 1, which implies that the DRI contributes significantly to the distributions. Again, the relative distributions in Figs. 4(c) and 4(d) show that the DES mechanism plays a more important role in the case of $\theta = 0°$, as the REDTI contributes more significantly to the case of $\theta = 90°$. The distribution in Fig. 4(c) is located in quadrant 1 and has a relatively large amplitude around the diagonal. In Fig. 4(d), it is located in quadrants 2 and 4 and has a small amplitude in quadrant 1. The single-electron momentum distribution in Fig. 4(e) for $\theta = 0°$ is also somewhat broader than that in Fig. 4(f) for $\theta = 90°$, in agreement with our analyses in Figs. 2(e) and 2(f). One can observe that for the case of the intermediate laser intensity, the results in Figs. 4(a)–4(d) are similar to the experimental ones for N_2 [26] obtained at $I \approx 1.2 \times 10^{14}$ W/cm^2.

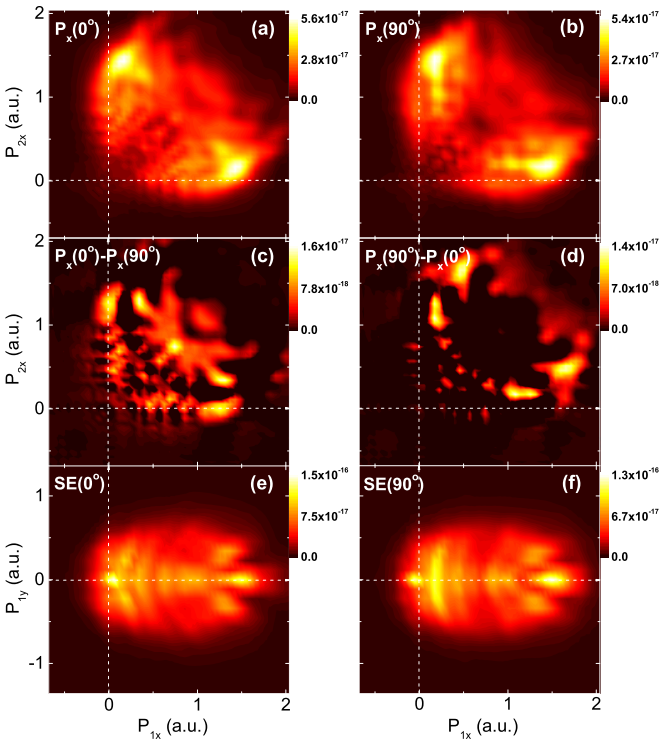

FIG. 5. (Color online) Same as Fig. 2, except $I = 2 \times 10^{14}$ W/cm^2. One can see that the maximal kinetic energy of the electron parallel to the laser polarization is about 1.15 a.u. for both $\theta = 0^\circ$ and 90° [see (a) and (b)]. That perpendicular to the laser polarization is about 0.11 a.u. for both $\theta = 0^\circ$ and 90° [see (e) and (f)].

C. High-intensity cases

For $I = 2 \times 10^{14}$ W/cm^2, the difference between the two angles $\theta = 0^\circ$ and $\theta = 90^\circ$ begins to diminish. The distributions in Figs. 5(a) and 5(b) are similar, and so are those in Figs. 5(c) and 5(d). They illustrate that one electron is at rest as the other leaves with larger momenta. As this remarkable phenomenon is believed to be closely associated with the DRI, the DES mechanism related to the escape of two electrons with a similar momentum can still be seen in Fig. 5(c). Accordingly, an extended analysis [by virtue of the relative distribution $|\phi_1(0^\circ)|^2 - |\phi_1(90^\circ)|^2$] indicates that the single-electron momentum distribution in Fig. 5(e) for $\theta = 0^\circ$ remains somewhat broader than that in Fig. 5(f) for $\theta = 90^\circ$. From Figs. 5(a) and 5(b), one can expect that at higher laser intensities, the structure of the molecule plays a smaller role in the DI.

V. EFFECTS OF TWO-CENTER INTERFERENCE

As the rescattering electron approaches the two cores of the molecule, it can be subjected to the effect of two-center interference [3]. The effect is remarkable for the parallel orientation [27,28]. For the perpendicular case, the molecule behaves similar to an atom, and the interference effect basically does not arise [45]. Due to the interference effect, the ratio of DI vs SI yields is always larger at $\theta = 90^\circ$ than that at $\theta = 0^\circ$, as shown in Fig. 1(b).

One can expect that the interference effect will be greatest if the rescattering electron falls into the molecular potential and recombines with the cores. This occurs in the DES process in which the rescattering electron is captured by the nuclei by exciting the second electron and forming a doubly excited state. As shown in Fig. 2, for low laser intensities, the DES process dominates in the DI of the parallel orientation. As a result, the DI yields at $\theta = 0^\circ$ will be influenced significantly by the interference effect. These above discussions shed light on why the DI yields at $\theta = 0^\circ$ are lower than those at $\theta = 90^\circ$ for the cases with low laser intensities in Fig. 1(a). For high laser intensities, the DRI and REDTI processes dominate in the DI. However, for these two processes, the rescattering electron skims over the cores instead of recombining with them, and therefore the interference effect is relatively weak compared with the DES process. As the SI yields at $\theta = 0^\circ$ are always larger than those at $\theta = 90^\circ$, the DI yields at $\theta = 0^\circ$ also prevail over those at $\theta = 90^\circ$ for the cases with high laser intensities in Fig. 1(a).

One of the limitations of our 2D model with the BO approximation is that the nuclear motion is neglected. Previous studies have shown that for one-dimensional H_2 molecules with relatively low laser intensities, the double ionization is always observed close to the equilibrium internuclear distance [15]. We therefore expect that the motions of the nuclei and the effect vibration states also have a small role in the orientation dependence of the molecular DI, especially for relatively low laser intensities at which the rescattering-induced NSDI mechanisms dominate in the DI. Specifically, the effect of two-center interference is closely associated with the internuclear distance and the orientation angle. In our cases of H_2, the interference effect appears for the parallel orientation in the rescattering process of DI and induces the suppression of the DI yields for the parallel molecule. As the nuclear motion is considered, the interference effect for the parallel molecule can change somewhat. But in comparison with the perpendicular molecule for which the interference effect disappears [45], the suppression of the DI yields for the parallel molecule arising from the interference effect does not change. The importance of two-center interference in the molecular HHG has been revealed in 2D simulations of H_2^+ with the BO approximation [3] and has been verified in experimental studies of CO_2 [46,47]. We therefore expect that the effect of two-center interference on the molecular DI, revealed in our simulations for H_2, will also appear for other molecules such as N_2 and CO_2, for which the Coulomb explosion cannot occur in the DI process.

To check our results, we have extended our simulations to other internuclear distances. The suppression of the DI yield for the parallel molecule, as shown in Fig. 1(b), occurs in all of our cases. Several typical results with $R = 1.7$ a.u. and $R = 1.9$ a.u. are shown in Fig. 6. Here, the effective charges of the 2D model Hamiltonian H_0 are adjusted so that the electronic energies of H_2 and H_2^+ at these two internuclear distances are similar to those used in Fig. 1. One can see that these results with different internuclear distances R in Fig. 6 are similar to those in Fig. 1, except for the cases at the low laser intensity of $I = 0.25 \times 10^{14}$ W/cm^2. It is interesting to note that the ratio of SI yields at $\theta = 0^\circ$ vs $\theta = 90^\circ$ is smaller than unity here, implying that the SI yield

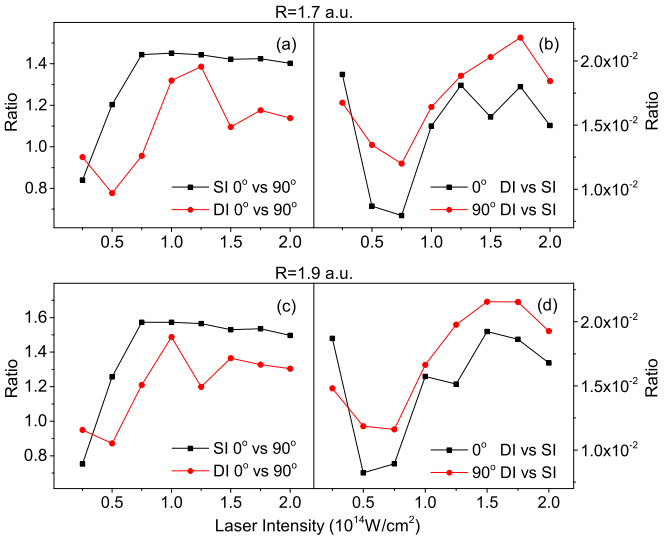

FIG. 6. (Color online) (a) and (c) The ratios of SI and DI yields at $\theta = 0^\circ$ vs $\theta = 90^\circ$ and (b) and (d) the ratios of DI vs SI yields at $\theta = 0^\circ$ and 90° for model H_2 with different laser intensities and internuclear distances. In (a) and (b), $R = 1.7$ a.u., and in (c) and (d), $R = 1.9$ a.u.

of the parallel molecule is lower than the perpendicular one. Accordingly, the ratio of DI vs SI yields at $\theta = 0^\circ$ is also higher than that at $\theta = 90^\circ$. The reason can be explained as follows. As discussed in Ref. [39], for strong laser fields, the Coulomb potential of the molecule is distorted significantly in the ionization process. As a result, two-center interference generally plays no role in ionization. However, as the laser intensity is low and the Coulomb potential is not influenced significantly, the interference effect indeed can induce the suppression of ionization for the parallel molecule. This first interference-induced minimum occurs at an electronic momentum of $p = \pi/(R\cos\theta)$ [35], which is smaller for larger internuclear distances. Because the main contributions to ionization come from the electron with low energy, the model H_2 molecules with similar ionization potentials are more easily affected by the interference effect for relatively larger internuclear distances.

Comparing these curves in Figs. 6(a) and 6(c), one can also arrive at the conclusion that the DI is more sensitive to the molecular structure than SI, in agreement with our analyses in Fig. 1. In Figs. 6(a) and 6(c), the curves with squares showing the ratio for SI are similar within a vertical scaling factor at different internuclear distances, but the curves with circles for DI differ significantly from each other.

We also simulate the DI of the N_2 molecule by adjusting the effective charges of H_0 at $R = 2.07$ a.u. so that the ground-state energy of the model system agrees with the real N_2 molecule, with $E_0(N_2) = -1.57$ a.u. and $E_0(N_2^+) = -1$ a.u. [28]. With higher ground-state electronic energies than H_2, the model N_2 molecule is easier to ionize, but the suppression of the DI yield at the parallel orientation can still be observed in our simulations, as shown in Fig. 7. For shorter laser pulses such as five-cycle 800-nm pulses, our other simulations show that this suppression phenomenon still appears. The results obtained are similar to those shown in Fig. 1, so we do not present them here. The above results suggest that this suppression phenomenon for DI arising from the interference effect can be general for molecules.

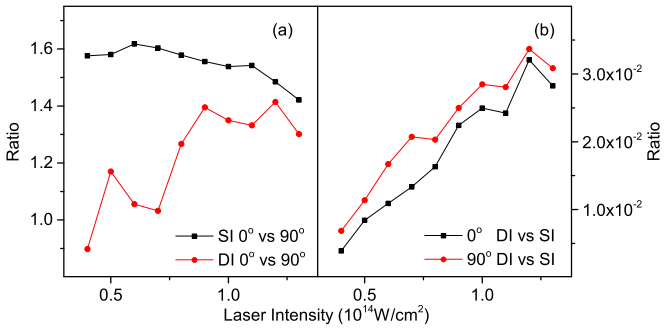

FIG. 7. (Color online) Same as Fig. 1, but for model N_2.

VI. EXTENDED DISCUSSION OF DIFFERENT NSDI MECHANISMS

It can be helpful to discuss the different NSDI mechanisms, which arise from the rescattering process and are used in our analyses in this paper. The main mechanisms for NSDI can be described as follows [30]. For high laser intensities, as the energy of the rescattering electron (the first electron) is large enough to release the bound electron (the second electron) directly, the mechanism of DRI for NSDI is expected. In this case, both electrons will be ejected along the same direction. For intermediate laser intensities, as the energy of the rescattering electron is not large enough to release the bound electron directly, it can excite the bound electron. Then, the excited electron is ionized by the laser field later. In this case, the mechanism of REDTI is expected, and these two electrons will appear in the laser field along opposite directions. For low laser intensities, the rescattering electron can be captured by the Coulomb potential by exciting the second electron and forming a doubly excited state. In this case, the mechanism of DES (i.e., recollision-induced doubly excited states) is expected, and these two electrons will appear in the laser field along the same direction as in the DRI case. The DES mechanism has been widely used in explaining relevant physical phenomena [26,30]. However, doubly excited states are difficult to trace directly as they decay very quickly in strong laser fields. Despite this difficulty, one can still anticipate that for DRI, since the second electron is released directly by the recollision of the first electron, both electrons are more likely to appear in the laser field with different momenta (similar to the result for elastic collision); for DES, since both electrons are located at excited states after the recollision and are ionized by the laser field later, they are more likely to exit the molecule with similar momenta.

In our simulations, for the parallel molecule, these two electrons show a preference to exit the molecular potential with similar momenta as the laser intensities are relatively low, as shown in Fig. 2(a). We thus expect that in this low-intensity case at which the energy of the rescattering electron is not large enough to release the second electron directly, the DES mechanism contributes significantly to NSDI. As the laser field is strong enough, the DRI mechanism dominates, and

the momenta of these two DI electrons differ significantly, as shown in Fig. 5(a).

It should be stressed that at high laser intensities, the mechanism of sequential ionization of these two electrons will dominate in the DI. However, in our simulations, due to the use of absorbing boundaries, sequential ionization cannot be described well. It has been shown that as the sequential ionization dominates, the motions of the nuclei have significant influence on the DI [48,49]. In addition, the magnetic effect is also important in DI [34]. Despite some limitations, our 2D simulations with the BO approximation indeed suggest that as the laser intensity increases, the difference in the DI at different orientation angles diminishes. We expect that this result is also applicable when the nuclear motion and the magnetic effect are considered.

VII. CONCLUSION

Using a 2D two-electron model, we have studied the double ionization of aligned H_2 at diverse laser intensities. Our simulations show that for the parallel orientation, the two electrons prefer to avoid each other laterally. As a result, they more easily stay in a doubly excited state formed through recollision and exit the molecular potential with similar momenta longitudinally. For the perpendicular orientation, the lateral movement is confined more strongly, and the two electrons tend to avoid each other longitudinally. Accordingly, they prefer to escape from the molecular potential at different times and leave the nuclei with different momenta along the laser polarization. The difference in the dynamics of DI at different angles diminishes as the laser intensity increases. The effect of two-center interference also significantly influences the DI yields of the molecule at the parallel orientation, especially for low laser intensities. We show that different DI mechanisms respond differently to the interference effect. These results are expected to shed light on the complex dynamics of DI from aligned molecules at the ultrafast time scale. Further research is also necessary for the full understanding of orientation-related DI phenomena of molecules.

ACKNOWLEDGMENTS

This work was supported by the National Natural Science Foundation of China (Grant No. 11274090) and the Fundamental Research Funds for the Central Universities (Grant No. GK201403002).

[1] P. B. Corkum, Phys. Rev. Lett. **71**, 1994 (1993).
[2] P. A. Franken, A. E. Hill, C. W. Peters, and G. Weinreich, Phys. Rev. Lett. **7**, 118 (1961).
[3] M. Lein, N. Hay, R. Velotta, J. P. Marangos, and P. L. Knight, Phys. Rev. Lett. **88**, 183903 (2002).
[4] P. Agostini and L. F. DiMauro, Rep. Prog. Phys. **67**, 813 (2004).
[5] P. B. Corkum and F. Krausz, Nat. Phys. **3**, 381 (2007).
[6] P. Agostini, F. Fabre, G. Mainfray, G. Petite, and N. K. Rahman, Phys. Rev. Lett. **42**, 1127 (1979).
[7] B. Yang, K. J. Schafer, B. Walker, K. C. Kulander, P. Agostini, and L. F. DiMauro, Phys. Rev. Lett. **71**, 3770 (1993).
[8] M. B. Gaarde, K. J. Schafer, K. C. Kulander, B. Sheehy, D. Kim, and L. F. DiMauro, Phys. Rev. Lett. **84**, 2822 (2000).
[9] A. l'Huillier, L. A. Lompre, G. Mainfray, and C. Manus, Phys. Rev. A **27**, 2503 (1983).
[10] B. Walker, B. Sheehy, K. C. Kulander, and L. F. DiMauro, Phys. Rev. Lett. **77**, 5031 (1996).
[11] D. Bauer, Phys. Rev. A **56**, 3028 (1997).
[12] C. Guo, M. Li, J. P. Nibarger, and G. N. Gibson, Phys. Rev. A **58**, R4271 (1998).
[13] M. Lein, E. K. U. Gross, and V. Engel, Phys. Rev. Lett. **85**, 4707 (2000).
[14] E. Eremina, X. Liu, H. Rottke, W. Sandner, M. G. Schätzel, A. Dreischuh, G. G. Paulus, H. Walther, R. Moshammer, and J. Ullrich, Phys. Rev. Lett. **92**, 173001 (2004).
[15] M. Lein, T. Kreibich, E. K. U. Gross, and V. Engel, Phys. Rev. A **65**, 033403 (2002).
[16] S. Baier, C. Ruiz, L. Plaja, and A. Becker, Phys. Rev. A **74**, 033405 (2006).
[17] J. S. Prauzner-Bechcicki, K. Sacha, B. Eckhardt, and J. Zakrzewski, Phys. Rev. Lett. **98**, 203002 (2007).
[18] D. F. Ye, X. Liu, and J. Liu, Phys. Rev. Lett. **101**, 233003 (2008).
[19] X. Wang and J. H. Eberly, Phys. Rev. Lett. **105**, 083001 (2010).
[20] W. Becker, X. Liu, P. J. Ho, and J. H. Eberly, Rev. Mod. Phys. **84**, 1011 (2012).
[21] S. X. Hu, Phys. Rev. Lett. **111**, 123003 (2013).
[22] R. Velotta, N. Hay, M. B. Mason, M. Castillejo, and J. P. Marangos, Phys. Rev. Lett. **87**, 183901 (2001).
[23] I. V. Litvinyuk, K. F. Lee, P. W. Dooley, D. M. Rayner, D. M. Villeneuve, and P. B. Corkum, Phys. Rev. Lett. **90**, 233003 (2003).
[24] Y. V. Vanne and A. Saenz, Phys. Rev. A **82**, 011403(R) (2010).
[25] S. Sukiasyan, C. McDonald, C. Destefani, M. Yu. Ivanov, and T. Brabec, Phys. Rev. Lett. **102**, 223002 (2009).
[26] D. Zeidler, A. Staudte, A. B. Bardon, D. M. Villeneuve, R. Dörner, and P. B. Corkum, Phys. Rev. Lett. **95**, 203003 (2005).
[27] C. Figueira deMorisson Faria, T. Shaaran, X. Liu, and W. Yang, Phys. Rev. A **78**, 043407 (2008).
[28] W. Li and J. Liu, Phys. Rev. A **86**, 033414 (2012).
[29] T. Brabec, M. Yu. Ivanov, and P. B. Corkum, Phys. Rev. A **54**, R2551(R) (1996).
[30] S. Baier, A. Becker, and L. Plaja, Phys. Rev. A **78**, 013409 (2008).
[31] H. Niikura, F. Légaré, R. Hasbani, M. Yu. Ivanov, D. M. Villeneuve, and P. B. Corkum, Nature (London) **421**, 826 (2003).
[32] A. S. Alnaser, T. Osipov, E. P. Benis, A. Wech, B. Shan, C. L. Cocke, X. M. Tong, and C. D. Lin, Phys. Rev. Lett. **91**, 163002 (2003).
[33] H. Niikura, F. Légaré, R. Hasbani, A. D. Bandrauk, M. Yu. Ivanov, D. M. Villeneuve, and P. B. Corkum, Nature (London) **417**, 917 (2002).
[34] E. Lötstedt and K. Midorikawa, Phys. Rev. A **87**, 013426 (2013).
[35] M. Lein, P. P. Corso, J. P. Marangos, and P. L. Knight, Phys. Rev. A **67**, 023819 (2003).

[36] K. C. Kulander, K. R. Sandhya Devi, and S. E. Koonin, Phys. Rev. A **25**, 2968 (1982).
[37] J. L. Krause, K. J. Schafer, and K. C. Kulander, Phys. Rev. A **45**, 4998 (1992).
[38] M. D. Feit, J. A. Fleck, Jr., and A. Steiger, J. Comput. Phys. **47**, 412 (1982).
[39] Y. J. Chen and B. Hu, Phys. Rev. A **81**, 013411 (2010).
[40] Y. J. Chen and B. Hu, J. Chem. Phys. **131**, 244109 (2009).
[41] C. R. Stia, O. A. Fojón, P. F. Weck, J. Hanssen, and R. D. Rivarola, J. Phys. B **36**, L257 (2003).
[42] A. Senftleben, O. Al-Hagan, T. Pflüger, X. Ren, D. Madison, A. Dorn, and J. Ullrich, J. Chem. Phys. **133**, 044302 (2010).
[43] Y. Li, J. Chen, S. P. Yang, and J. Liu, Phys. Rev. A **76**, 023401 (2007).
[44] B. Feuerstein, R. Moshammer, D. Fischer, A. Dorn, C. D. Schröter, J. Deipenwisch, J. R. Crespo Lopez-Urrutia, C. Höhr, P. Neumayer, J. Ullrich, H. Rottke, C. Trump, M. Wittmann, G. Korn, and W. Sandner, Phys. Rev. Lett. **87**, 043003 (2001).
[45] Y. Chen, Y. Li, S. Yang, and J. Liu, Phys. Rev. A **77**, 031402(R) (2008).
[46] T. Kanai, S. Minemoto, and H. Sakai, Nature (London) **435**, 470 (2005).
[47] C. Vozzi, F. Calegari, E. Benedetti, J.-P. Caumes, G. Sansone, S. Stagira, M. Nisoli, R. Torres, E. Heesel, N. Kajumba, J. P. Marangos, C. Altucci, and R. Velotta, Phys. Rev. Lett. **95**, 153902 (2005).
[48] X. M. Tong and C. D. Lin, Phys. Rev. A **70**, 023406 (2004).
[49] S. Saugout, E. Charron, and C. Cornaggia, Phys. Rev. A **77**, 023404 (2008).